Hyperglycemia-induced cathepsin L maturation: Implications for diabetic comorbidities and COVID-19 susceptibility

Qiong He[1,*], Miao-Miao Zhao[1,*✉], Ming-Jia Li[1], Xiao-Ya Li[1], Jian-Min Jin[2,3], Ying-Mei Feng[4], Li Zhang[5], Wei-Jin Huang[5], Fang-Yuan Yang[1], and Jin-Kui Yang[1✉]

[1]Department of Endocrinology, Beijing Diabetes Institute, Beijing Tongren Hospital, Capital Medical University, Beijing, China

[2]Department of Respiratory and Critical Care Medicine, Beijing Tongren Hospital, Capital Medical University, Beijing, China

[3]Department of Internal Medicine, Union Hospital, Tongji Medical College, Huazhong University of Science and Technology, Wuhan 430022, China.

[4]Department of Science and Technology, Beijing Youan Hospital, Capital Medical University, Beijing, China

[5]Division of HIV/AIDS and Sex-Transmitted Virus Vaccines, Institute for Biological Product Control, National Institutes for Food and Drug Control (NIFDC), Beijing, China

[*]These authors contributed equally.

✉Correspondence to Jin-Kui Yang (jkyang@ccmu.edu.cn) or Miao-Miao Zhao (mmzhao@ccmu.edu.cn).

ABSTRACT

Diabetes is the second most frequent chronic comorbidity for COVID-19 mortality, yet the underlying mechanism remains unclear. Previous studies suggest that Cathepsin L (CTSL) is implicated in diabetic complications such as nephropathy and retinopathy. Our previous research identified CTSL as a critical protease that promotes SARS-CoV-2 infection and a potential drug target. Here, we show that individuals with diabetes have elevated blood CTSL levels, which facilitates SARS-CoV-2 infection. Chronic hyperglycemia, as indicated by HbA1c levels, is positively correlated with CTSL concentration and activity in diabetic patients. Acute hyperglycemia induced by a hyperglycemic clamp in healthy individuals increases CTSL activity. *In vitro*, high glucose, but not high insulin, promotes SARS-CoV-2 infection in wild-type (WT) cells, while *CTSL* knockout (KO) cells show reduced susceptibility to high glucose-promoted effects. Using lung tissue samples from diabetic and non-diabetic patients, as well as db/db diabetic and control mice, our findings demonstrate that diabetic conditions increase CTSL activity in both humans and mice. Mechanistically, high glucose levels promote CTSL maturation and CTSL translocation from the endoplasmic reticulum (ER) to the lysosome via the ER-Golgi-lysosome axis. This study emphasizes the significance of hyperglycemia-induced cathepsin L maturation in the development of diabetic comorbidities and complications.

Introduction

Cysteine proteases, including cathepsin L (CTSL), are crucial in human pathobiology due to their diverse biological activities inside and outside cells. Recent studies suggest that cathepsins, including CTSL, play a role in metabolic disorders such as obesity and diabetes (Crawford et al., 2022; Ding et al., 2020; Limonte et al., 2022), as well as diabetic complications. In previous studies, CTSL has been linked to proteinuria in podocytes (Reiser et al., 2004) and intraocular angiogenesis (Shimada et al., 2010), making it a potential target for diabetic nephropathy and vision-threatening diseases such as proliferative diabetic retinopathy (Shimada et al., 2010). Selective inhibition of CTSL may hold potential for therapeutic interventions.

More recently, CTSL has been implicated in the cleavage and processing of the SARS-CoV-2 spike protein, which is necessary for the virus to enter and replicate in host cells, as reported by our group (Zhao et al., 2021b) and others (Jackson et al., 2022; Muralidar et al., 2021). Our previous studies show that elevated CTSL concentrations are associated with increased disease severity and CTSL is crucial for activation of all emerging SARS-CoV-2 variants, making it a potential drug target for future mutation-resistant therapy (Zhao et al., 2021b; Zhao et al., 2022). However, the role of CTSL in COVID-19 infection among diabetic patients has not been explored.

Patients with diabetes have been identified as a high-risk group for developing severe COVID-19 and experiencing increased mortality rates (Khunti et al., 2021). Several studies have reported that patients with diabetes are 1.23 - 5.87 times more likely to experience severe COVID-19 and death compared to those without diabetes (Dennis et al., 2021; Shi et al., 2020; Williamson et al., 2020). According to data from the American Centers for Disease Control and Prevention (CDC), diabetes is the second leading chronic comorbidity contributing to COVID-19 deaths, after hypertension . Even among patients with diabetes,

after full adjustment, those with higher blood glucose (HbA1c ≥ 7.5%) had higher hazard ratio (HR) (1.95 *vs.* 1.31) than those with lower blood glucose (HbA1c < 7.5%) (Williamson et al., 2020).

This study investigates, for the first time, the impact of high glucose levels on CTSL maturation and diabetic comorbidities and complications, with a focus on SARS-CoV-2 infection in patients with diabetes. Our findings suggest that high glucose levels promote CTSL maturation and translocation from the endoplasmic reticulum to the lysosome, potentially contributing to diabetic comorbidities and complications.

Results

Diabetic COVID-19: severe, high CTSL

In COVID-19 patients, we conducted a case-control study to examine the association of diabetes and COVID-19 severity in 207 COVID-19 inpatients from two hospitals. We matched 62 patients by gender and age, 31 with diabetes and 31 without (Fig. 1a). Supplementary Table 1 summarizes the demographic and clinical characteristics of these diabetic and non-diabetic COVID-19 patients. We found that diabetic patients had a significantly higher risk of developing severe COVID-19 than non-diabetic patients according to the clinical classification criteria (*http://www.nhc.gov.cn/*), and had more symptoms such as fever, cough, fatigue, and dyspnea (Fig. 1b). Diabetic COVID-19 patients showed higher levels of inflammation and infection markers (Supplementary Table 1). These results suggest that diabetes is strongly associated with severity of COVID-19.

To explore the mechanisms of hyperglycemia and SARS-CoV-2 infection, we collected plasma samples from Beijing Youan Hospital on Day 0 (the admission day), Day 14, and Day 28 after discharge from the hospital (Fig. 1c). SARS-CoV-2 infects host cells through

the virus spike protein binding with ACE2 receptor. It uses host proteases, such as CTSL and cathepsin B (CTSB) to activate its spike protein by cleavage, which enhances its cell entry (Jackson et al., 2022; Muralidar et al., 2021). We measured the plasma levels of COVID-19 related proteins, ACE2, CTSL, and CTSB in diabetic and non-diabetic COVID-19 patients. Only CTSL levels were significantly higher in diabetic patients than in non-diabetic patients and changed with the course of COVID-19. CTSL peaked on admission day and decreased significantly after discharge from the hospital (Fig. 1d-f). These results indicate that CTSL is strongly associated with COVID-19, as previously reported (Zhao et al., 2022), and may be involved in diabetes in COVID-19 patients.

Impact of hyperglycemia on CTSL activity

In non-COVID-19 participants, we investigated the correlation of CTSL with chronic and acute hyperglycemia using two studies. First, to examine the impact of chronic hyperglycemia on CTSL, we performed a case-control study in 61 patients with type 2 diabetes and 61 euglycemic subjects, matched for sex and age (Supplementary Table 2). We found that plasma CTSL activity and concentration were strongly positively correlated with chronic hyperglycemia indicated by HbA1c, and were significantly higher in diabetic patients than in euglycemic individuals (Fig. 2a-d). Second, to examine the impact of acute hyperglycemia on CTSL, we performed a hyperglycemic clamp study in 15 healthy male subjects (Fig. 2e-g). We observed that CTSL activity increased parallelly with blood glucose levels (Fig. 2h, i). However, CTSL concentration did not change with blood glucose levels (Fig. 2j). Therefore, chronic hyperglycemia is strongly associated with both CTSL concentration and activity, while acute hyperglycemia only affects CTSL activity.

We also observed a strongly correlation between CTSL activity/concentration and other chronic comorbidities like hypertensin and coronary heart disease (CHD), except for

diabetes (Supplementary Table 3). Additionally, elevated blood glucose levels also accompanied with an increase in insulin and proinsulin C-peptide levels in acute hyperglycemic individuals (Fig. 2f, g) and diabetic patients (insulin resistance) (Gerich, 2003). It is unclear whether the increased CTSL activity/concentration is solely a result of hyperglycemia or the corresponding hyperinsulinemia, and further clarification is needed.

Glucose enhances SARS-CoV-2 via CTSL

To validate our hypothesis that diabetic patients are more susceptible to SARS-CoV-2 infection results from higher CTSL levels, we conducted *in vitro* experiments using a SARS-CoV-2 pseudovirus system, which indicates the virus invasion rate instead of replication, and utilized the SARS-CoV-2 susceptible human hepatoma cell line Huh7, given that the liver is a primary target of SARS-CoV-2 (Gupta et al., 2020).

First, to examine if cells cultured with serum from diabetic patients are more susceptible to SARS-CoV-2 infection, we compared the infectivity of cells cultured with healthy and diabetic sera exposed to SARS-CoV-2 using a luciferase assay. The results showed that cells cultured with diabetic serum had higher infection rate than cultured with healthy serum (Fig. 3a), indicating diabetic serum facilitated SARS-CoV-2 entry into host cells.

Next, we investigated whether elevated blood glucose or insulin level promoted SARS-CoV-2 infection by culturing Huh7 cells in cell media with various concentrations of glucose or insulin. Consistent with our clinical data, the results showed that infection was more severe in Huh7 cells at high glucose levels, while insulin levels had a minimal impact on SARS-CoV-2 infection (Fig. 3b, c).

Given that hyperglycemia increased CTSL levels (Fig. 2) and facilitated SARS-CoV-2 entry into host cells (Fig. 3b), we hypothesized that high blood glucose promoted SARS-CoV-2 infection through CTSL. To investigate the requirement of CTSL in

SARS-CoV-2 infection, we used the CRISPR-Cas9 system to establish a stable *CTSL* knockout (KO) Huh7 cell line. The knockout efficiency of CTSL protein of *CTSL* KO Huh7 cell line was confirmed in Fig. 3d. Compared with wild-type (WT) cells, knockout of *CTSL* led to a significant reduction in SARS-CoV-2 infection (Fig. 3e), suggesting that CTSL is crucial for SARS-CoV-2 infection as we previously reported (Zhao et al., 2022).

We then conducted a *CTSL* KO Huh7 cell infection experiment under different glucose conditions, to illustrate the impact of glucose level on SARS-CoV-2 infection via CTSL. The results showed that WT Huh7 cell cultured in high glucose medium exhibited a much higher infective rate than those in low glucose medium. However, *CTSL* KO Huh7 cells maintained a low infective rate of SARS-CoV-2 regardless of glucose or insulin levels (Fig. 3f-h). Therefore, hyperglycemia enhanced SARS-CoV-2 infection dependent on CTSL. Considering that CTSL realizes its proteolytic function through its enzyme activity and protein concentration, subsequent studies aimed to reveal whether the CTSL activity or concentration changed under high glucose condition.

High glucose boosts CTSL activity

To investigate the impact of hyperglycemia on CTSL activity, we conducted a series experiments. Our findings showed that elevated glucose levels significantly stimulated both intracellular and extracellular CTSL activity in a dose-dependent manner in Huh7 cells (Fig. 4a, b), which was consistent with our clinical data (Fig. 2a, h). In contrast, insulin levels had no effect on CTSL activity in Huh7 cells (Fig. 4c, d), indicating that it was hyperglycemia, rather than hyperinsulinemia, that boosted CTSL activity in diabetic patients.

We then evaluated CTSL activity in human and mouse biopsy tissues under high blood glucose condition. The demographic and clinical information for the human lung tissue samples donors in this study can be found in Supplementary Table 4. Diabetic mice (db/db

mice) had significantly increased glucose, body weight and fasting insulin levels compared to control (db/m mice) group (Fig. 4e-g). We observed an elevation of CTSL activity in both diabetic mice and human lung tissues (Fig. 4h, i), suggesting that high glucose condition may increase CTSL activity in the respiratory system in diabetic patients and mice *in vivo*. The increase of CTSL activity in diabetic mice liver tissue (Fig. 4h) was consistent with the results of Huh7 hepatocytes (Fig. 4a).

High glucose stimulates CTSL maturation

To investigate the impact of high blood glucose on CTSL expression, we first measured the mRNA levels of CTSL under different glucose concentrations using D-glucose and L-glucose (Supplementary Fig. 1). While D-glucose is commonly used as a major energy source, L-glucose cannot be absorbed by cells but has similar physical properties to D-glucose, making it an ideal control. Surprisingly, our results showed that glucose or insulin levels did not affect CTSL mRNA levels in Huh7 cells, mouse tissues or human tissues (Supplementary Fig. 1), indicating that glucose did not influence CTSL transcription.

CTSL undergoes several forms during its translation and post-translational maturation process. The immature pro-cathepsin L (proCTSL, 39 kDa) possesses an N-terminal proregion, which acts as an autoinhibitor. The protein is translocated through the endoplasmic reticulum (ER)-Golgi apparatus-lysosome axis, and the proregion is removed in the acidic environment in lysosome results in either single chain mature cathepsin L (sc-mCTSL, 31 kDa) or double chain mature cathepsin L (dc-mCTSL, 24 kDa) (Fig. 5a) (Coutinho et al., 2012; Ishidoh and Kominami, 2002; Reiser et al., 2010). Only mature CTSL in lysosome has catalytic activity against specific substrates, while proCTSL does not (Ishidoh and Kominami, 2002).

Interestingly, we found that high glucose levels promoted CTSL maturation, whereas

insulin had no effect on this process, as shown in Fig. 5b. Our results indicated that high D-glucose levels reduced proCTSL and increased sc-mCTSL and dc-mCTSL in a glucose dose-dependent manner (Fig. 5b, Supplementary Fig. 2). The results also confirmed that only D-glucose induced CTSL maturation from proCTSL to mCTSL, while L-glucose had no such effects (Fig. 5b, c). Similar effects of high glucose on CTSL maturation were also observed in diabetic mice and human tissues compared with their healthy counterparts (Fig. 5d, e). These results suggested that hyperglycemia rather than hyperinsulinemia or other physical parameters associated with CTSL maturation. This was consistent with our previous data that elevated glucose levels enhanced CTSL activity (Fig. 4a), since only mature CTSL has enzymatic activity.

High glucose promotes CTSL translocation

We have shown that high glucose promoted CTSL maturation by converting proCTSL into mCTSL (Fig. 5, Supplementary Fig. 2). However, the mechanism underlying this process remained unclear. As mentioned previously, CTSL maturation depends on structural activation via the ER-Golgi apparatus-lysosome axis and acid activation at low pH environment (Fig. 6a) (Ishidoh and Kominami, 2002; Reiser et al., 2010). Only the CTSL in lysosome is processed into mature form and has proteolytic activity, while the CTSL in the ER or Golgi apparatus is immature and does not have enzymatic activity. Based on this, we hypothesized that high blood glucose may drive CTSL maturation via the ER-Golgi apparatus-lysosome axis. We labeled specific proteins in each organelle: calreticulin for ER, GM130 for Golgi apparatus and lamp1 for lysosome (Supplementary Fig. 3). We also confirmed CTSL expression in Huh7 cells (Supplementary Fig. 4). Confocal microscopy results revealed that under low glucose conditions, CTSL tended to co-localize within the ER rather than lysosomes (Fig. 6b, e). This finding suggests that CTSL primarily existed in

an immature form under low glucose conditions. As glucose level increased, CTSL in the Golgi apparatus remained unchanged (Fig. 6c, f), while co-localized largely increased in the lysosomes (Fig. 6d, g), suggesting CTSL predominantly existed in mature form under high glucose conditions. Therefore, we concluded that high glucose facilitated CTSL translocation through the ER-Golgi apparatus-lysosome axis.

Discussion

Almost immediately after the SARS-CoV-2 emerged, it became apparent that individuals with chronic conditions, including diabetes, were disproportionately affected, with a heightened risk of hospitalization and mortality (Williamson et al., 2020). Diabetes may increase susceptibility to severe SARS-CoV-2 infections for various suggested reasons. These include higher viral titer, relatively low functioning T lymphocytes that lead to decreased viral clearance, vulnerability to hyperinflammation and cytokine storm syndrome, and comorbidities associated with type 2 diabetes, such as cardiovascular disease, non-alcoholic fatty liver disease, hypertension, and obesity (Mazucanti and Egan, 2020; Moradi-Marjaneh et al., 2021). Additionally, other risk factors that may contribute to the severity of infection include increased expression of angiotensin-converting enzyme 2 (ACE2) (Rao et al., 2020) and furin (Fernandez et al., 2018). However, most current studies on COVID-19 and diabetes focus on epidemiological evidence and biomarker features, but few investigate the causal link and underlying mechanisms of how hyperglycemia enhances SARS-CoV-2 infection, confirmed by human body fluids, biopsies, and animal models. The underlying mechanisms by which diabetes or hyperglycemia exacerbates COVID-19 remain to be fully elucidated.

This study identified that CTSL maturation induced by hyperglycemia may contribute to the higher mortality and severity of COVID-19 in patients with diabetes. Our clinical data

showed that human plasma CTSL activity and concentration were strongly correlated with acute (in euglycemic participants under high glucose clamp conditions) and chronic (in diabetic patients, both with and without COVID-19) hyperglycemia, respectively. Using lung tissue samples from diabetic and non-diabetic patients, as well as db/db diabetic and control mice, we found that diabetic conditions increased CTSL activity in both humans and mice. High glucose promoted SARS-CoV-2 infection in WT cells, while *CTSL* KO cells showed reduced susceptibility to high glucose promoting effects. Mechanistically, we proposed that hyperglycemia promoted CTSL maturation by accelerating its translocation from the ER to lysosome via Golgi apparatus. This condition increased the functionality of CTSL, which cleaved the spike protein of SARS-CoV-2, promoting virus membrane fusion and infection (Fig. 6h).

To date, there have been limited studies investigating the relationship between cathepsin maturation and glucose. In 1998, Tournu C, et al. reported that D-glucose did not impact mRNA levels for CTSB or CTSL or secretion of proCTSL. However, D-glucose did significantly enhance the amount of mature forms of CTSB and CTSL (Tournu et al., 1998). More recently, Shi Q, et al. found that increased glucose metabolism promotes O-GlcNAcylation of the lysosome-encapsulated protease CTSB, leading to elevated levels of mature CTSB in macrophages and secretion in the tumor microenvironment (Shi et al., 2022). These findings support our evidence that hyperglycemia drives CTSL maturation and enhances SARS-CoV-2 infection.

ACE2 has previously been identified as a critical host cell surface receptor that enables SARS-CoV-2 entry into host cells (Wrapp et al., 2020). While some studies have reported that glucose can increase ACE2 expression in cell lines (Hardtner et al., 2013), numerous other studies have found that ACE2 is downregulated in diabetic patients (Mizuiri et al., 2008; Reich et al., 2008). Garreta et al. recently conducted a study using a human kidney

organoid system to investigate the impact of diabetes on SARS-CoV-2 infections. The study revealed that hyperglycemia enhanced SARS-CoV-2 infection and hyperglycemic human kidney organoids had elevated ACE2 levels (Garreta et al., 2022). Therefore, it remains controversial whether diabetes results in up- or downregulation of ACE2. In our study, we evaluated plasma levels of ACE2, CTSL, and CTSB in COVID-19 patients with and without diabetes. We found that only CTSL levels were significantly increased in diabetic patients compared to non-diabetic patients and varied during the course of COVID-19.

In addition to CTSL, there may be other bioactive factors involved in mediating SARS-CoV-2 infection in patients with diabetes. A recent study revealed that diabetic patients have lower levels of serum 1,5-anhydro-D-glucitol (1,5-AG), a small-molecule metabolite in human blood that exhibits potent antiviral activity against SARS-CoV-2. The reduced levels of 1,5-AG have been associated with increased viral loads and severe respiratory tissue damage caused by SARS-CoV-2. Mechanistically, the study found that 1,5-AG binds directly to the S2 subunit of the spike protein, which disrupts virus-host membrane fusion and inhibits infection (Tong et al., 2022). Therefore, we propose that diabetes may promote COVID-19 infection through multiple factors, and CTSL is only one of several important factors.

Apart from diabetes, other comorbidities such as hypertension and CHD are also prevalent in COVID-19 patients. Interestingly, our study revealed a strong correlation between CTSL activity and concentration with hypertension and CHD in these patients. Using an angiotensin II-induced hypertension model, researchers observed an increase in blood pressure and CTSL activity (Lu et al., 2020). Whether these chronic comorbidities contribute to increased morbidity and mortality of COVID-19 by increasing CTSL activity and concentration requires further investigation in the future.

In conclusion, our study demonstrates that hyperglycemia drives the maturation and

activation of CTSL, for only mature form of CTSL gains its function of proteolysis. Therefore, targeting CTSL may be a promising therapeutic strategy for diabetic comorbidities and complications.

Materials and methods

Detailed methods include the following:

- KEY RESOURCES TABLE
- RESOURCE AVAILABILITY
  - Lead Contact
  - Materials Availability
  - Data and Code Availability
- EXPERIMENTAL MODELS AND SUBJECT DETAILS
  - Patients and clinical samples
  - Experimental mice
  - Cell lines and reagents
- METHOD DETAILS
  - Detection of SARS-Cov-2 entry related host biomarkers
  - Production of pseudovirus
  - Pseudovirus infection *in vitro*
  - Establishment of *CTSL*-KO Huh7 cell line via CRISPR/Cas 9
  - Generation of *CTSL*-KO monoclonal Huh7 cell line
  - RNA extraction and quantitative real-time PCR analyses
  - Intraperitoneal glucose tolerance test
  - Western blot analysis
  - Analysis of CTSL activity

- Immunofluorescence assay

- QUANTIFICATION AND STATISTICAL ANALYSIS

Key resources table

Reagent or resource	Source	Identifier
Antibodies		
CTSL	R&D System	AF952
α-tubulin	Proteintech	66031-1-Ig
β-actin	Proteintech	66009-1-Ig
Calreticulin	Cellsignal	112238
GM130	BD Biosciences	610822
Lamp1 Goat IgG	PTM BIO Beyotime	PTM-5775 A7007
Rabbit IgG	Beyotime	A7016
Mouse IgG	Beyotime	A7028
Bacterial and virus strains		
G*ΔG-VSV	Kerafast	Cat#EH1020-PM
Biological samples		
Blood samples from patients with COVID-19	Beijing Youan Hospital, Capital Medical University; Wuhan Union Hospital, Huazhong University of Science and Technology	N/A
Blood samples from healthy individuals	Beijing Youan Hospital, Capital Medical University; Beijing Tongren Hospital, Capital Medical University	N/A
Chemicals, peptides, and recombinant proteins		
Ac-FR-AFC	R&D	Cat. No ES009
TransScript First-Strand cDNA Synthesis SuperMix	Transgen	Cat. No AT301
TransStart Tip Green qPCR SuperMix	Transgen	Cat. No AQ141
Critical commercial assays		
Human ACE2 Elisa kit	Cloud-Clone Corp	Cat. No L220216094
Human CTSL ELISA Kit	Elabscience	Cat. No E-EL-H0671
Human CTSB ELISA kit	Elabscience	Cat. No E-EL-H6151
Mouse insulin ELISA kit	Millipore	Cat. No EZRMI-13K
Britelite Plus Kit	Perkinelmer	Cat. No 6066761
Cell Counting Kit	Transgen	Cat. No FC101-04
RNAprep Pure Cell/ Bacteria kit	Tiangen	Cat. No DP430
RNAprep Pure Tissue kit	Tiangen	Cat. No DP431
Deposited data		

Demographic and clinical characteristics of patients	Beijing Youan Hospital, Capital Medical University; Wuhan Union Hospital, Huazhong University of Science and Technology; Beijing Tongren Hospital, Capital Medical University	N/A
Experimental models: Cell lines		
The Huh7 (Homo sapiens, liver) cell line	Cell Resource Center, Chinese Academy of Medical Sciences	N/A
Experimental models: Organisms/strains		
db/db mice	Vital River Laboratories	N/A
db/m mice	Vital River Laboratories	N/A
Human lung samples	Beijing Youan Hospital, Capital Medical University	N/A
Oligonucleotides		
Primer: CTSL (human) - F: AAACTGGGAGGCTTATCTCACT	Beijing Biolino CO.,LTD	N/A
Primer: CTSL (human) - R: GCATAATCCATTAGGCCACCAT	Beijing Biolino CO.,LTD	N/A
Primer: CTSL (mouse) - F: CTACACAACGGGGAATACAGC	Beijing Biolino CO.,LTD	N/A
Primer: CTSL (mouse) - R: CATTGGTCATGTCACCGAAGG	Beijing Biolino CO.,LTD	N/A
Primer: β-actin (human) – F: TCATGAAGTGTGACGTGGACATC	Beijing Biolino CO.,LTD	N/A
Primer: β-actin (human) – R: CAGGAGGAGCAATGATCTTGATCT	Beijing Biolino CO.,LTD	N/A
Primer: β-actin (mouse) – F: GTGACGTTGACATCCGTAAAGA	Beijing Biolino CO.,LTD	N/A
Primer: β-actin (mouse) – R: GCCGGACTCATCGTACTCC	Beijing Biolino CO.,LTD	N/A
Recombinant DNA		
N/A	N/A	N/A
Software and algorithms		
Image J	Image J Software	https://imagej.net/software/imagej/
Graphpad prism 7.0	GraphPad Software	https://www.graphpad.com
SPSS for Windows 17.0	IBM SPSS Software	https://www.ibm.com/analytics/spss-statistics-software
Microsoft Office Home and Student 2019	Microsoft Corporation	https://www.microsoft.com/microsoft-365
Other		

N/A	N/A	N/A

Experimental model and study participant details

Patients and clinical samples

The study protocol was approved by the Ethics Committee of Beijing Tongren Hospital, Capital Medical University (TRECKY2020-013, TRECKY2021-202). The retrospective cohort study included 207 COVID-19 patients from two hospitals. 120 adult COVID-19 inpatients admitted to Wuhan Union Hospital, Huazhong University of Science and Technology (Wuhan, China) between January 29 and March 20, 2020. Another 87 consecutive COVID-19 inpatients were hospitalized at Beijing Youan Hospital, Capital Medical University (Beijing, China) between January 21 and April 30, 2020. 31 COVID-19 patients with diabetes and 31 COVID-19 patients without diabetes were matched for gender and age and included in the final analysis. The clinical features are presented in Supplementary Table 1. SARS-CoV-2 was detected in respiratory specimens using real-time RT-PCR, following the protocol recommended by the World Health Organization. COVID-19 was classified into four categories: mild, moderate, severe and critical, according to the clinical classification criteria (http://www.nhc.gov.cn/). Patients from Beijing Youan Hospital, Capital Medical University were further followed up. They experienced a mean of 14 days of hospitalization and were followed up on the 14th day (Day 14) and 28th day (Day 28) after discharge from the hospital. Blood samples were collected shortly after the admission to the hospital (Day 0) and on Day 14 and Day 28. Demographic, clinical, and laboratory data were extracted from the electronic hospital information system using a standardized form.

Another total of 122 age- and gender-matched diabetic and non-diabetic volunteers without COVID-19 were recruited in Beijing Tongren Hospital, Capital Medical University.

Blood samples were collected after overnight fasting for the determination of CTSL activity and concentration and other biochemical parameters. All biochemical measurements have participated in the Chinese Ministry of Health Quality Assessment Program. The demographic and clinical characteristics are shown in Supplementary Table 2.

Human lung tissue samples were obtained from 6 patients who underwent lung surgery at Beijing Tongren Hospital between March and June, 2022. The baseline characteristics are presented in Supplementary Table 4.

The plasma samples of hyperglycemic clamp study were from a previously conducted clinical trial (NCT03972215). Fifteen healthy male research subjects were received a 160-min hyperglycemic clamp study with a baseline blood glucose level + 6.9 mmol/L as the target level. Blood samples were obtained at intervals throughout the clamp study. The plasma was collected and stored at -80℃ until use.

Experimental mice

The study used 10-week-old db/db mice as diabetic mode and db/m mice as their healthy control, maintained on a KBS background. All mice were obtained from Vital River Laboratories (Beijing, China). The mice were housed at constant humidity and temperature, with a 12h light/dark cycle. The protocols for the use of mice were approved by the Ethical Review Committee at the Institute of Zoology, Capital Medical University.

Cell lines and reagents

The Huh7 (*Homo sapiens*, liver) cell line (Cell Resource Center, Chinese Academy of Medical Sciences, Beijing, China), was maintained in high glucose Dulbecco's modified Eagle's medium (DMEM) (Sigma-Aldrich, St. Louis, MO, USA) supplemented with streptomycin (100 mg/ml), penicillin (100 units/ml), and fetal bovine serum (10%, Gibco, Carlsbad, CA). The cells were maintained at 37°C in a humidified atmosphere of 5% CO2

and 95% air.

Method details

Detection of SARS-CoV-2 entry related host biomarkers

Plasma samples of patients with COVID-19 at Day 0, Day 14, and Day 28 were collected and stored at −80 °C within 2 h. The samples were analyzed using commercially available enzyme-linked immunosorbent assays (ELISA) following the manufacturer's instructions. All samples were detected without virus inactivation to retain the original results in a P2 + biosafety laboratory. ACE2 was measured using the Human ACE2 Elisa kit (Cloud-Clone Corp, Cat. No L220216094). CTSL and CTSB were measured using the Human CTSL ELISA Kit (Elabscience, Cat. No E-EL-H0671) and Human CTSB ELISA kit (Elabscience, Cat. No E-EL-H6151). The kits were designed for usage with human serum or plasma samples and showed no cross-reactions.

Production of pseudovirus

The SARS-CoV-2 pseudovirus were generated with the incorporation of SARS-CoV-2 spike protein (SARS-2-S) into vesicular stomatitis virus (VSV)-based pseudovirus system. The pseudoviruses used in the current study have been validated in previous studies (Lv et al., 2020; Whitt, 2010). For this VSV-based pseudovirus system, the backbone was provided by VSV-G pseudotyped virus (G*ΔG-VSV) that packages expression cassettes for firefly luciferase instead of VSV-G in the VSV genome (Nie et al., 2020). Therefore, the luciferase activity of VSV phosphoprotein (VSV-P) were used for indicators of pseudovirus infection.

Pseudovirus infection *in vitro*

Huh7 cells were plated in 96-well plates and allowed to adhere until they reached 70% confluency. Subsequently, these cells were cultured with different medium or serum obtained from diabetic or euglycemic individuals as indicated. Following this, the cells were

infected with SARS-CoV-2 pseudovirus at 1.3×10^4 $TCID_{50}$/ml at 37 °C. After coincubation with pseudovirus of 24 hours, the activities of firefly luciferases were measured on cell lysates using luciferase substrate, Britelite Plus Kit (Perkinelmer, Cat. No 6066761) according to the manufacturer's instructions. The firefly luciferase activity was measured rapidly using a luminometer (Turner BioSystems, USA) as described previously (Yang et al., 2017). Cell viability were measured by CCK assay using Cell Counting Kit (Transgen, Cat. No FC101-04). The infection rates were adjusted by cell viability.

Establishment of *CTSL*-KO Huh7 cell line via CRISPR/Cas9

To produce the *CTSL*-KO cell line, we utilized CRISPR/Cas9 technology. The single guide RNA (sgRNA) was designed using the Zhang Lab Guide Design Resources (https://zlab.bio/guide-design-resources) tool. The sgRNA scaffold was commercially obtained from Sangon, with the sequence designed as 5'-CTTTGTGGACATCCCTAAGC-3'. For sgRNA and Cas9 protein to enter into Huh7 cell, electroporation-mediated transfection was performed. First, 4×10^5 Huh7 cells were centrifuged and re-suspended in 10 μL of Buffer R following the manufacturer's instructions (Invitrogen, USA) for electroporation. Next, Cas9 protein (1 μg) and sgRNA (0.2 μg) were added to each sample and mixed gently (Cas9 protein: sgRNA at a 1:1 molar ratio). Huh7 cells were electroporated for 5 times to minimize the *CTSL* gene on a Neon Transfection device (Invitrogen, USA).

Generation of *CTSL*-KO monoclonal Huh7 cell line

Cells were isolated from the stable *CTSL*-KO Huh7 cell pool by trypsinization and any cell clumps were broken up into individual cells. Cells concentration was quantitated in this homogenized cell solution with a cell counter. Then, 100 μL of the 5 cells/mL solution was transferred into each well of a 96-well plate. By doing this, the average density of 0.5 cells/well of the plate was seeded. Seeding an average of 0.5 cells/well ensured that some

wells received a single cell, while minimizing the likelihood that any well receives more than one cell. Then we observed and recorded the cell growth in the plate for the following 30 days. Once the cells have expanded but before they become over-confluent, we trypsinized the cells and expanded them to larger culture dishes.

RNA extraction and quantitative real-time PCR analyses

Total RNA was extracted and purified from the cultured Huh7 cells, human and mouse tissues using RNAprep Pure Cell/ Bacteria kit (Tiangen, Cat. No DP430) and RNAprep Pure Tissue kit (Tiangen, Cat. No DP431) according to the manufacturer's instructions. RNA (0.5 μg) was reverse transcribed to cDNA in a final volume (20 μL) using TransScript First-Strand cDNA Synthesis SuperMix (Transgen, Cat. No AT301). RT-PCR analyses were performed with TransStart Tip Green qPCR SuperMix (Transgen, Cat. No AQ141). Gene expression values were normalized to the control (β-actin) level. Supplementary Table 5 provides a list of all primer sequences. Quantitative real-time PCR (qRT-PCR) and data collection were done on a LightCycler 96 system (Roche, Switzerland).

Intraperitoneal glucose tolerance test (IPGTT)

The db/db and db/m mice were subjected to an overnight fast lasting 16 hours, during which they were permitted unrestricted access to water. Subsequently, they received an intraperitoneal injection of 1 g/kg body weight glucose. Blood samples were obtained at 0, 15-, 30-, 60-, and 120-minutes post-glucose injection. Blood glucose levels were determined using an automatic glucometer (One Touch, LifeScan, USA), while insulin concentrations were evaluated using a highly sensitive mouse insulin ELISA kit (Millipore, Cat. No EZRMI-13K), according to the manufacturer's instructions.

Western blot analysis

Total protein was extracted from Huh7 cells and human and mouse tissues. The protein amount was assessed using the BCA protein assay kit (Thermo, Cat. No WH333441).

Samples of 30-50 μg of protein were separated by SDS-PAGE, transferred to PVDF membrane (Millipore, Cat. No 0000167358), and detected using enhanced chemiluminescent reaction (Zhao et al., 2021a). The antibody information was summarized in Supplementary Table 6.

Analysis of CTSL activity

The activity of CTSL in plasma, human and mouse tissues, Huh7 cells and cell medium was evaluated using its specific substrate, Ac-FR-AFC (R&D, Cat. No ES009). Prior to measurement, the cell medium was concentrated using the ultra-tube (Milipore, Cat. No UFC501096). The test samples were evaluated in the presence of a reaction buffer (100mM NaAc, 5mM EDTA, pH 5.3). The reaction was conducted in 100 μL system (50μL sample containing CTSL protein+ 47μL reaction buffer + 1 μL DTT (1 mM) + 2 μL substrate Ac-FR-AFC (10 mM)) in 96-well black plates. The plated was cultured at 37℃ for 2 h in light avoidance incubator. The fluorescence emitted from the samples was then measured using a fluorescence plate reader (Infinite 200, TECAN, China) at the Ex = 380 nm, Em = 460 nm wavelengths.

Immunofluorescence assay

The CTSL, calreticulin, Golgi membrane protein 130 (GM130) and lysosomal associated membrane protein 1 (Lamp 1) distributions in the Huh7 cells were visualized by immunofluorescent staining. The CTSL, calreticulin, GM130 and Lamp1 antibody species source IgG were used as negative control (Supplementary Fig. 3). Briefly, Huh7 cells was cultured in 35mm confocal dishes after poly-l-lysine coating. After high/low glucose treatment for 96 h, Huh7 cells were then fixed by 4% paraformaldehyde (PFA) and permeabilized by a detergent 0.25% triton X-100. A specific primary antibody is applied on the Huh7 cell surface at 4 ℃ overnight. After wash out, the secondary antibody is applied

at room temperature for 1 hour avoid from light. All pictures were captured under Laser Scanning Confocal Microscopy (FV3000RS, Olympus, Japan). The antibodies information was summarized in Supplementary Table 6.

Quantification and statistical analysis

Clinical data are shown as percentage or median, as appropriate. Comparison of continuous data between two independent groups was performed using the Mann–Whitney *U*-test. An unpaired *t* test was used for comparing the averages/means of two independent or unrelated groups. A paired t-test was used to test whether the mean difference between pairs of measurements is existing. Analysis of variance (ANOVA) was used for checking if the means of two or more categories are significantly different from each other. Spearman's rho test (two-tailed) was used to analyze nonparametric correlations of parameters correlated with CTSL levels and diabetes. Fluorescence intensity was calculated by Plot Profile tool in Image J software. Graphpad prism 7.0 software and SPSS for Windows 17.0 were used for statistical analysis, with statistical significance set at two-sided. $^{*}P < 0.05$, $^{**}P < 0.01$, $^{***}P < 0.001$, $^{****}P < 0.0001$.

Acknowledgment

We thank participants and staff of the case-control studies for their valuable contributions. This work was supported by grants from National Natural Science Foundation of China (81930019), Beijing Municipal Administration of Hospitals Clinical Medicine Development of Special Funding Support (ZYLX201823) to J.K.Y.

Author contributions

J.K.Y. conceived the idea for the study, designed the experiments and wrote the final manuscript. Q.H. and M.M.Z. designed and performed the experiments and wrote the first draft of the manuscript. M.J.L. and X.Y.L. performed pseudovirus assays and immunofluorescence assays. J.M.J., Y.M.F., F.Y.Y. and M.M.Z. collected the clinical data.

L.Z. and W.J.H. partially participated the pseudovirus assays.

Lead Contact

The data that support the findings of this study are available from the Leading Contact, Dr. Jin-Kui Yang (jkyang@ccmu.edu.cn).

Conflict of interests

The authors declare no competing interests.

Materials Availability

All the unique reagents generated in this study are available from the Lead Contact with a completed Materials Transfer Agreement.

Supplementary information

Figure S1 to S4

Table S1 to S6

References

Chronic comorbidities contributing to COVID-19 deaths. Data from the American Centers for Disease Control and Prevention (CDC), as of April, 16, 2023. https://www.cdc.gov/nchs/nvss/vsrr/covid_weekly/index.htm#Comorbidities.

Coutinho, M.F., Prata, M.J., and Alves, S. (2012). Mannose-6-phosphate pathway: a review on its role in lysosomal function and dysfunction. Mol Genet Metab *105*, 542-550.

Crawford, S.A., Wiles, T.A., Wenzlau, J.M., Powell, R.L., Barbour, G., Dang, M., Groegler, J., Barra, J.M., Burnette, K.S., Hohenstein, A.C., *et al.* (2022). Cathepsin D Drives the Formation of Hybrid Insulin Peptides Relevant to the Pathogenesis of Type 1 Diabetes. Diabetes *71*, 2793-2803.

Dennis, J.M., Mateen, B.A., Sonabend, R., Thomas, N.J., Patel, K.A., Hattersley, A.T., Denaxas, S., McGovern, A.P., and Vollmer, S.J. (2021). Type 2 Diabetes and COVID-19-Related Mortality in the Critical Care Setting: A National Cohort Study in England, March-July 2020. Diabetes Care *44*, 50-57.

Ding, L., Goossens, G.H., Oligschlaeger, Y., Houben, T., Blaak, E.E., and Shiri-Sverdlov, R. (2020). Plasma cathepsin D activity is negatively associated with hepatic insulin sensitivity in overweight and obese humans. Diabetologia *63*, 374-384.

Fernandez, C., Rysa, J., Almgren, P., Nilsson, J., Engstrom, G., Orho-Melander, M., Ruskoaho, H., and Melander, O. (2018). Plasma levels of the proprotein convertase furin and incidence of diabetes and mortality. J Intern Med *284*, 377-387.

Garreta, E., Prado, P., Stanifer, M.L., Monteil, V., Marco, A., Ullate-Agote, A., Moya-Rull, D.,

Vilas-Zornoza, A., Tarantino, C., Romero, J.P., *et al.* (2022). A diabetic milieu increases ACE2 expression and cellular susceptibility to SARS-CoV-2 infections in human kidney organoids and patient cells. Cell Metab *34*, 857-873 e859.

Gerich, J.E. (2003). Contributions of insulin-resistance and insulin-secretory defects to the pathogenesis of type 2 diabetes mellitus. Mayo Clin Proc *78*, 447-456.

Gupta, A., Madhavan, M.V., Sehgal, K., Nair, N., Mahajan, S., Sehrawat, T.S., Bikdeli, B., Ahluwalia, N., Ausiello, J.C., Wan, E.Y., *et al.* (2020). Extrapulmonary manifestations of COVID-19. Nat Med *26*, 1017-1032.

Hardtner, C., Morke, C., Walther, R., Wolke, C., and Lendeckel, U. (2013). High glucose activates the alternative ACE2/Ang-(1-7)/Mas and APN/Ang IV/IRAP RAS axes in pancreatic beta-cells. Int J Mol Med *32*, 795-804.

Ishidoh, K., and Kominami, E. (2002). Processing and activation of lysosomal proteinases. Biol Chem *383*, 1827-1831.

Jackson, C.B., Farzan, M., Chen, B., and Choe, H. (2022). Mechanisms of SARS-CoV-2 entry into cells. Nat Rev Mol Cell Biol *23*, 3-20.

Khunti, K., Knighton, P., Zaccardi, F., Bakhai, C., Barron, E., Holman, N., Kar, P., Meace, C., Sattar, N., Sharp, S., *et al.* (2021). Prescription of glucose-lowering therapies and risk of COVID-19 mortality in people with type 2 diabetes: a nationwide observational study in England. Lancet Diabetes Endocrinol *9*, 293-303.

Limonte, C.P., Valo, E., Drel, V., Natarajan, L., Darshi, M., Forsblom, C., Henderson, C.M., Hoofnagle, A.N., Ju, W., Kretzler, M., *et al.* (2022). Urinary Proteomics Identifies Cathepsin D as a Biomarker of Rapid eGFR Decline in Type 1 Diabetes. Diabetes Care *45*, 1416-1427.

Lu, Y., Sun, X., Peng, L., Jiang, W., Li, W., Yuan, H., and Cai, J. (2020). Angiotensin II-Induced vascular remodeling and hypertension involves cathepsin L/V- MEK/ERK mediated mechanism. Int J Cardiol *298*, 98-106.

Lv, Z., Deng, Y.Q., Ye, Q., Cao, L., Sun, C.Y., Fan, C., Huang, W., Sun, S., Sun, Y., Zhu, L., *et al.* (2020). Structural basis for neutralization of SARS-CoV-2 and SARS-CoV by a potent therapeutic antibody. Science *369*, 1505-1509.

Mazucanti, C.H., and Egan, J.M. (2020). SARS-CoV-2 disease severity and diabetes: why the connection and what is to be done? Immun Ageing *17*, 21.

Mizuiri, S., Hemmi, H., Arita, M., Ohashi, Y., Tanaka, Y., Miyagi, M., Sakai, K., Ishikawa, Y., Shibuya, K., Hase, H., *et al.* (2008). Expression of ACE and ACE2 in individuals with diabetic kidney disease and healthy controls. Am J Kidney Dis *51*, 613-623.

Moradi-Marjaneh, R., Asgharzadeh, F., Khordad, E., and Marjaneh, M.M. (2021). Diabetes and COVID-19; a Review of Possible Mechanisms. Curr Pharm Des *27*, 2522-2527.

Muralidar, S., Gopal, G., and Visaga Ambi, S. (2021). Targeting the viral-entry facilitators of SARS-CoV-2 as a therapeutic strategy in COVID-19. J Med Virol *93*, 5260-5276.

Nie, J., Li, Q., Wu, J., Zhao, C., Hao, H., Liu, H., Zhang, L., Nie, L., Qin, H., Wang, M., *et al.* (2020). Establishment and validation of a pseudovirus neutralization assay for SARS-CoV-2. Emerging microbes & infections *9*, 680-686.

Rao, S., Lau, A., and So, H.C. (2020). Exploring Diseases/Traits and Blood Proteins Causally Related to Expression of ACE2, the Putative Receptor of SARS-CoV-2: A Mendelian Randomization Analysis Highlights Tentative Relevance of Diabetes-Related Traits. Diabetes Care *43*, 1416-1426.

Reich, H.N., Oudit, G.Y., Penninger, J.M., Scholey, J.W., and Herzenberg, A.M. (2008). Decreased

glomerular and tubular expression of ACE2 in patients with type 2 diabetes and kidney disease. Kidney Int *74*, 1610-1616.

Reiser, J., Adair, B., and Reinheckel, T. (2010). Specialized roles for cysteine cathepsins in health and disease. J Clin Invest *120*, 3421-3431.

Reiser, J., Oh, J., Shirato, I., Asanuma, K., Hug, A., Mundel, T.M., Honey, K., Ishidoh, K., Kominami, E., Kreidberg, J.A., *et al.* (2004). Podocyte migration during nephrotic syndrome requires a coordinated interplay between cathepsin L and alpha3 integrin. J Biol Chem *279*, 34827-34832.

Shi, Q., Shen, Q., Liu, Y., Shi, Y., Huang, W., Wang, X., Li, Z., Chai, Y., Wang, H., Hu, X., *et al.* (2022). Increased glucose metabolism in TAMs fuels O-GlcNAcylation of lysosomal Cathepsin B to promote cancer metastasis and chemoresistance. Cancer Cell *40*, 1207-1222 e1210.

Shi, Q., Zhang, X., Jiang, F., Zhang, X., Hu, N., Bimu, C., Feng, J., Yan, S., Guan, Y., Xu, D., *et al.* (2020). Clinical Characteristics and Risk Factors for Mortality of COVID-19 Patients With Diabetes in Wuhan, China: A Two-Center, Retrospective Study. Diabetes Care *43*, 1382-1391.

Shimada, N., Ohno-Matsui, K., Iseki, S., Koike, M., Uchiyama, Y., Wang, J., Yoshida, T., Sato, T., Peters, C., Mochizuki, M., *et al.* (2010). Cathepsin L in bone marrow-derived cells is required for retinal and choroidal neovascularization. Am J Pathol *176*, 2571-2580.

Tong, L., Xiao, X., Li, M., Fang, S., Ma, E., Yu, X., Zhu, Y., Wu, C., Tian, D., Yang, F., *et al.* (2022). A glucose-like metabolite deficient in diabetes inhibits cellular entry of SARS-CoV-2. Nat Metab *4*, 547-558.

Tournu, C., Obled, A., Roux, M.P., Deval, C., Ferrara, M., and Bechet, D.M. (1998). Glucose controls cathepsin expression in Ras-transformed fibroblasts. Arch Biochem Biophys *360*, 15-24.

Whitt, M.A. (2010). Generation of VSV pseudotypes using recombinant DeltaG-VSV for studies on virus entry, identification of entry inhibitors, and immune responses to vaccines. J Virol Methods *169*, 365-374.

Williamson, E.J., Walker, A.J., Bhaskaran, K., Bacon, S., Bates, C., Morton, C.E., Curtis, H.J., Mehrkar, A., Evans, D., Inglesby, P., *et al.* (2020). Factors associated with COVID-19-related death using OpenSAFELY. Nature *584*, 430-436.

Wrapp, D., Wang, N., Corbett, K.S., Goldsmith, J.A., Hsieh, C.L., Abiona, O., Graham, B.S., and McLellan, J.S. (2020). Cryo-EM structure of the 2019-nCoV spike in the prefusion conformation. Science *367*, 1260-1263.

Yang, W., Wang, J., Chen, Z., Chen, J., Meng, Y., Chen, L., Chang, Y., Geng, B., Sun, L., Dou, L., *et al.* (2017). NFE2 Induces miR-423-5p to Promote Gluconeogenesis and Hyperglycemia by Repressing the Hepatic FAM3A-ATP-Akt Pathway. Diabetes *66*, 1819-1832.

Zhao, M.M., Lu, J., Li, S., Wang, H., Cao, X., Li, Q., Shi, T.T., Matsunaga, K., Chen, C., Huang, H., *et al.* (2021a). Berberine is an insulin secretagogue targeting the KCNH6 potassium channel. Nat Commun *12*, 5616.

Zhao, M.M., Yang, W.L., Yang, F.Y., Zhang, L., Huang, W.J., Hou, W., Fan, C.F., Jin, R.H., Feng, Y.M., Wang, Y.C., *et al.* (2021b). Cathepsin L plays a key role in SARS-CoV-2 infection in humans and humanized mice and is a promising target for new drug development. Signal Transduct Target Ther *6*, 134.

Zhao, M.M., Zhu, Y., Zhang, L., Zhong, G., Tai, L., Liu, S., Yin, G., Lu, J., He, Q., Li, M.J., *et al.* (2022). Novel cleavage sites identified in SARS-CoV-2 spike protein reveal mechanism for cathepsin L-facilitated viral infection and treatment strategies. Cell Discov *8*, 53.

1

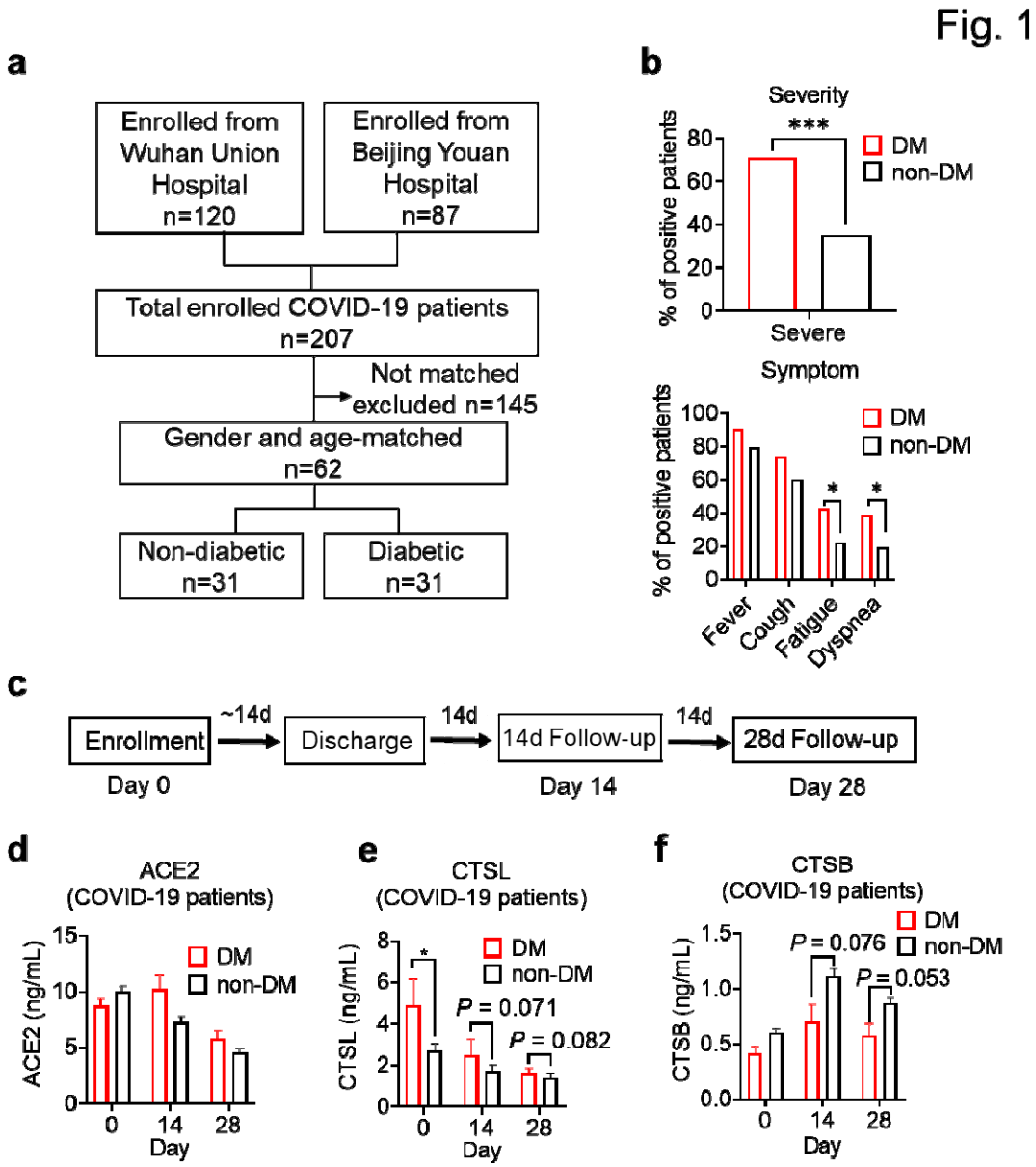

Fig. 1 Disease severity and CTSL levels in COVID-19 patients with and without diabetes. **a** Design and inclusion flowchart of the case-control study. Out of 207 COVID-19 patients from two hospitals, 62 were included in the study after matching for gender and age, 31 with diabetes and 31 without. **b** Comparison of symptom severity and prevalence between diabetic and non-diabetic COVID-19 patients. **c** Study design and timeline of the enrollment and follow-up study. After admitted to the hospital (Day 0), patients were hospitalized for a mean duration of 14 days, followed up 14 days (Day 14) and 28 days (Day 28) after discharge, and blood samples were collected at each time point. **d-f** Plasma levels of COVID-19 related proteins were measured in diabetic and non-diabetic COVID-19 patients on Day 0, Day 14, and Day 28. Statistical significance was assessed by unpaired *t*-test (**b**) and Mann-Whitney *U*-test (**d-f**). The data are presented as the means ± SEM. *$P < 0.05$, ***$P < 0.001$.

Fig. 2

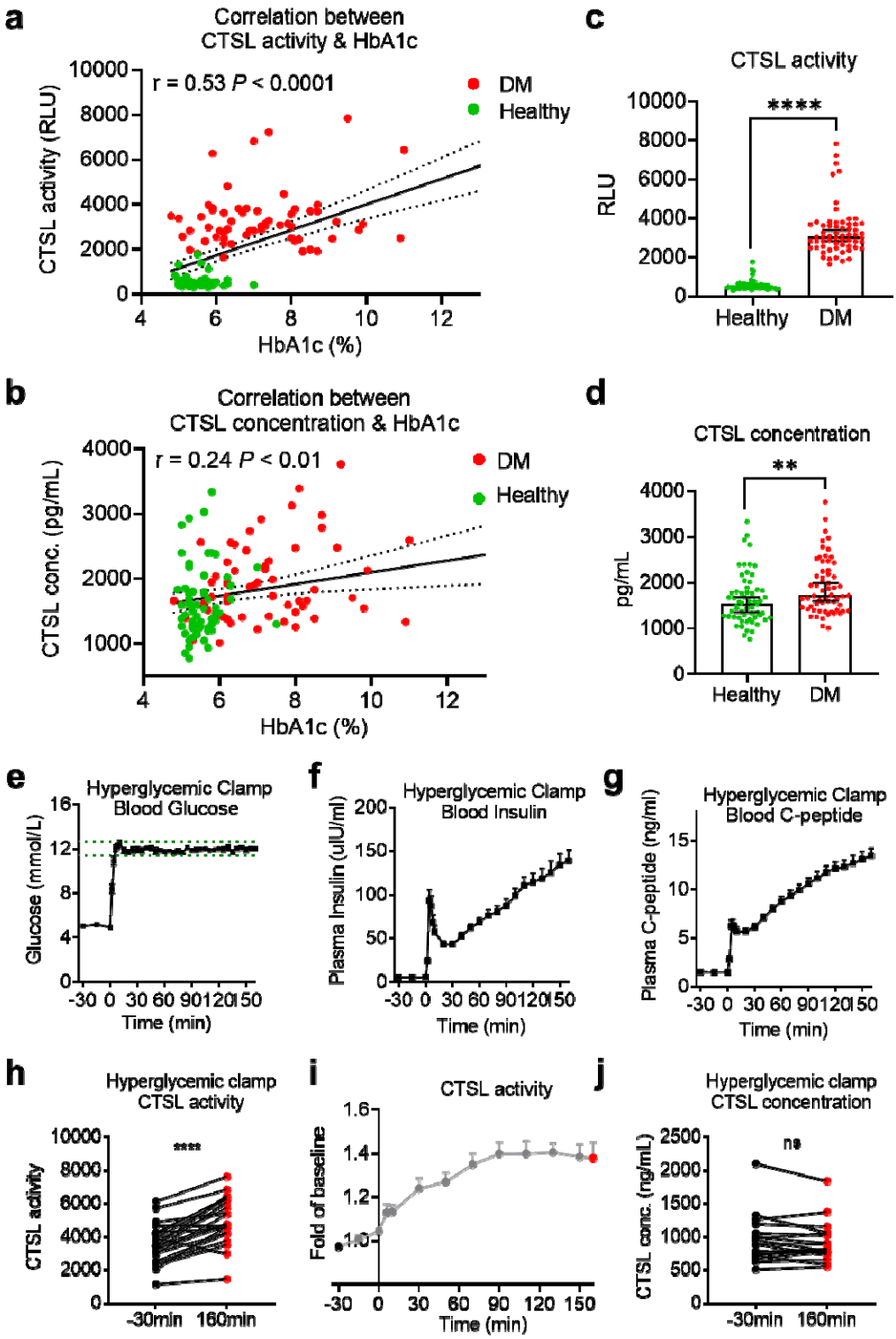

Fig. 2 Impact of chronic and acute hyperglycemia on CTSL concentration and activity.

a-d Effects of chronic hyperglycemia on CTSL activity and concentration in 122 gender- and age-matched individuals without COVID-19, including 61 euglycemic volunteers and 61 diabetic patients.

a Correlation between plasma CTSL activity and blood glucose level indicated by HbA1c. **b** Correlation between plasma CTSL concentration and HbA1c. The dashed line represents the 95% CI in **a** and **b**. **c** Comparison of plasma CTSL activity between the euglycemic and diabetic groups. **d** Comparison of plasma CTSL concentration between the euglycemic and diabetic groups. The data are presented as the median with 95% CI in **c** and **d**. **e**-**g** Hyperglycemic clamp study performed in 15 healthy male subjects. **e** Plasma glucose levels in subjects throughout the clamp study. The dashed lines represent the range of ± 5% of the hyperglycemic target level, i.e., basal blood glucose level + 6.9 mmol/L. **f** Insulin levels and **g** proinsulin C-peptide levels throughout the clamp study. **h**-**j** Effects of acute hyperglycemia on CTSL concentration and activity in 15 healthy male volunteers. **h** Plasma CTSL activity at the beginning and the end of the clamp study. **i** Plasma CTSL activity throughout the clamp study. **j** Plasma CTSL concentration at the beginning and the end of the clamp study. Statistical significance was assessed by Spearman correlation analysis (**a** and **b**), unpaired *t*-test (**c** and **d**) and paired *t*-test (**h** and **j**). The data are presented as the means ± SEM. $^{**}P < 0.01$, $^{****}P < 0.0001$.

Fig. 3

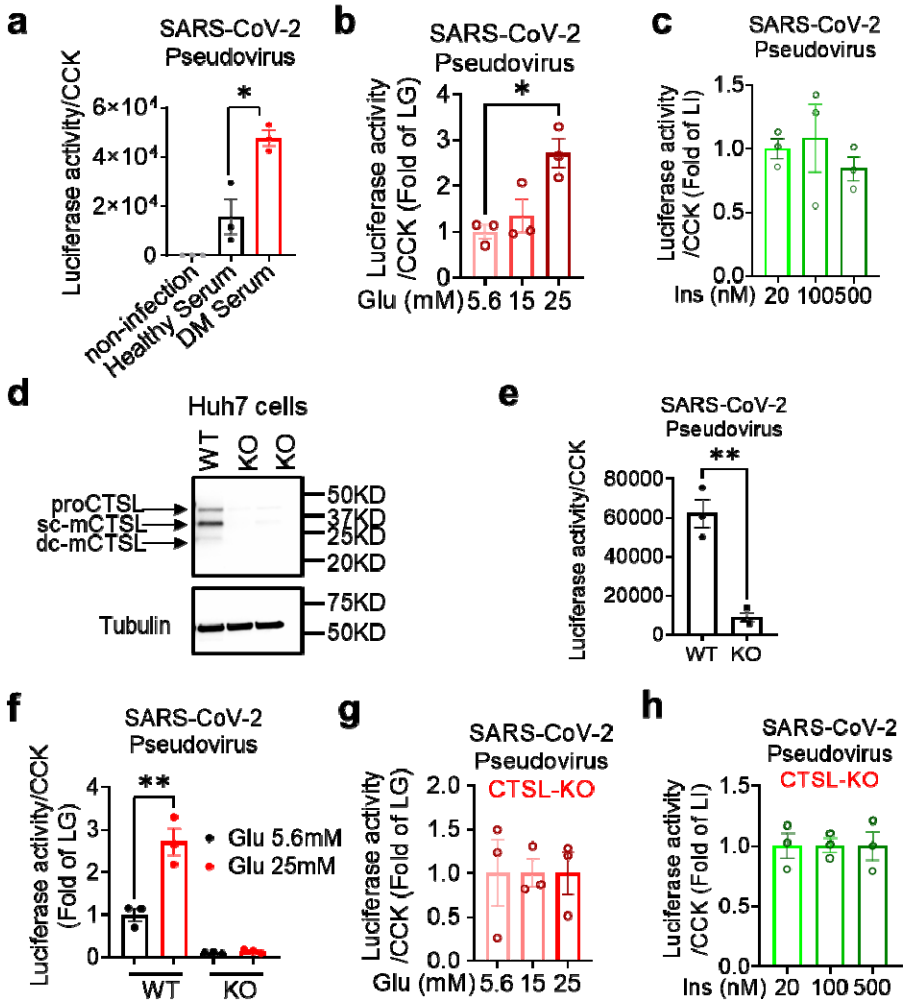

Fig. 3 Hyperglycemia enhances SARS-CoV-2 infection through CTSL.

Huh7 cells were infected with SARS-CoV-2 pseudovirus. **a** Wildtype (WT) cells cultured in sera from healthy and diabetic individuals were infected with SARS-CoV-2 pseudovirus (1.3×10^4 $TCID_{50}$/ml). Non-infected cells are used as control. The infection levels, as indicated by luciferase activities, were adjusted by cell viability, as indicated by CCK (n = 3). **b** The SARS-CoV-2 infection rate of WT cells after being cultured in different doses of glucose (5.6 mM, 15 mM and 25 mM) (n = 3). **c** The SARS-CoV-2 infection rate of WT cells after being cultured in different doses of insulin (20 nM, 100 nM and 500 nM) (n = 3). **d** Comparison of CTSL expression in WT and *CTSL* knockout (KO) cell lines. **e-h** The SARS-CoV-2 pseudovirus infection of WT and *CTSL* KO cells. **e** The SARS-CoV-2 infection rate of WT and *CTSL* KO cells (n = 3). **f** The SARS-CoV-2 infection rate of WT and *CTSL* KO Huh7 cells cultured in different doses of glucose (5.6 mM and 25 mM) (n = 3). **g** The SARS-CoV-2 infection rate of *CTSL* KO Huh7 cells cultured in different doses of glucose (5.6 mM, 15 mM and 25 mM) (n = 3). **h** The SARS-CoV-2 infection rate of *CTSL* KO Huh7 cells cultured in different doses of insulin (20 nM, 100 nM and 500 nM) (n = 3). Statistical significance was assessed by one-way ANOVA with Tukey's post hoc test (**a-c**, **g** and **h**) and Mann-Whitney U-test (**e** and **f**). The data are presented as the means ± SEM. *$P < 0.05$, **$P < 0.01$.

Fig. 4

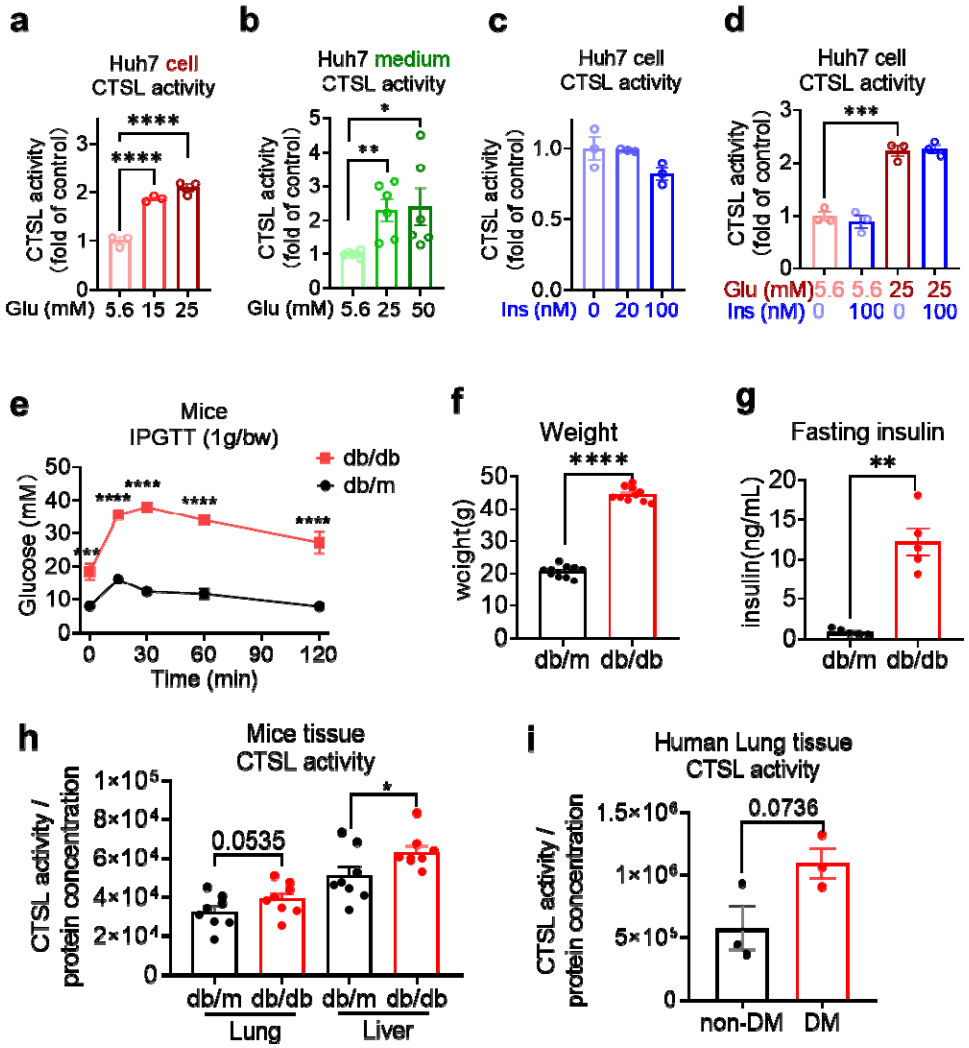

Fig. 4 Elevation of glucose levels enhance CTSL activity.

Effects of high glucose levels on CTSL activity in Huh7 cells, as well as in biopsy samples of mice and diabetic patients. **a** Intracellular CTSL activity was measured in Huh7 cells cultured in different glucose concentrations as indicated (n = 3). **b** Extracellular CTSL activity was measured in Huh7 cells cultured in different glucose concentrations as indicated (n = 6). **c** Intracellular CTSL activity was measured in Huh7 cells cultured in different insulin concentration as indicated (n = 3). **d** Intracellular CTSL activity was measured in Huh7 cells cultured in different glucose and insulin concentrations as indicated (n = 3). **e** The blood glucose levels during the intraperitoneal glucose tolerance test (IPGTT) in db/db diabetic and db/m control mice (n = 5). **f** Body weight of db/db and db/m mice was measured (n = 10). **g** Fasting insulin levels were measured in db/db and db/m mice (n = 5). **h** CTSL activity was measured in the lung and liver biopsy samples of db/db and db/m mice (n = 8). **i** CTSL activity was measured in human lung biopsy samples from diabetic (DM) and non-diabetic patients (n = 3). Statistical significance was assessed by one-way ANOVA with Tukey's post hoc test (**a**-**d**) and unpaired t-test (**e**-**i**). The data are presented as the means ± SEM. *P < 0.05, **P < 0.01, ***P < 0.001, ****P < 0.0001.

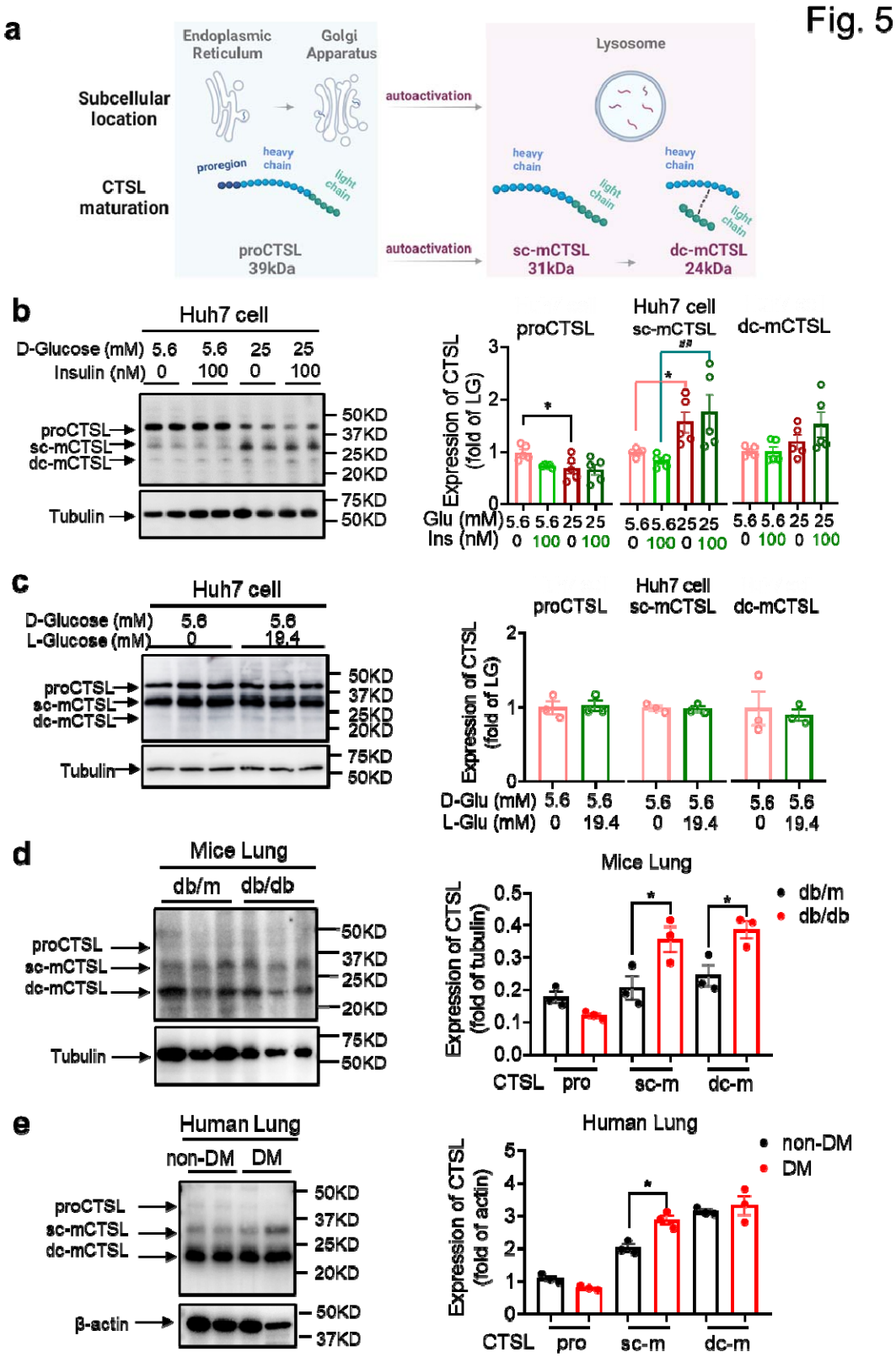

Fig. 5 High glucose levels stimulate CTSL maturation.

a Schematic of the CTSL maturation process. Pro-cathepsin L (ProCTSL, 39 kDa) in endoplasmic

reticulum (ER) and Golgi apparatus translocated to the lysosome and autoactivated into the single chain mature cathepsin L (sc-mCTSL, 31 kDa) and double chain mature cathepsin L (dc-mCTSL, 24KDa). **b** Western blot analysis of CTSL protein in Huh7 cells cultured with different doses of D-glucose and insulin as indicated (n = 5). **c** Western blot analysis of CTSL protein in Huh7 cells cultured with 5.6 mM D-glucose or D-glucose plus 19.4 mM L-glucose as indicated (n = 3). **d** Western blot analysis of CTSL protein in lung tissues from db/db and db/m mice (n = 3). **e** Western blot analysis of CTSL protein in human lung tissues from non-diabetic and diabetic patients (n = 3). Statistical significance was assessed by one-way ANOVA with Tukey's post hoc test (**b**) and Mann-Whitney U-test (**c**-**e**). The data are presented as the means ± SEM. $^{*}P < 0.05$, $^{\#\#}P < 0.01$.

Fig. 6

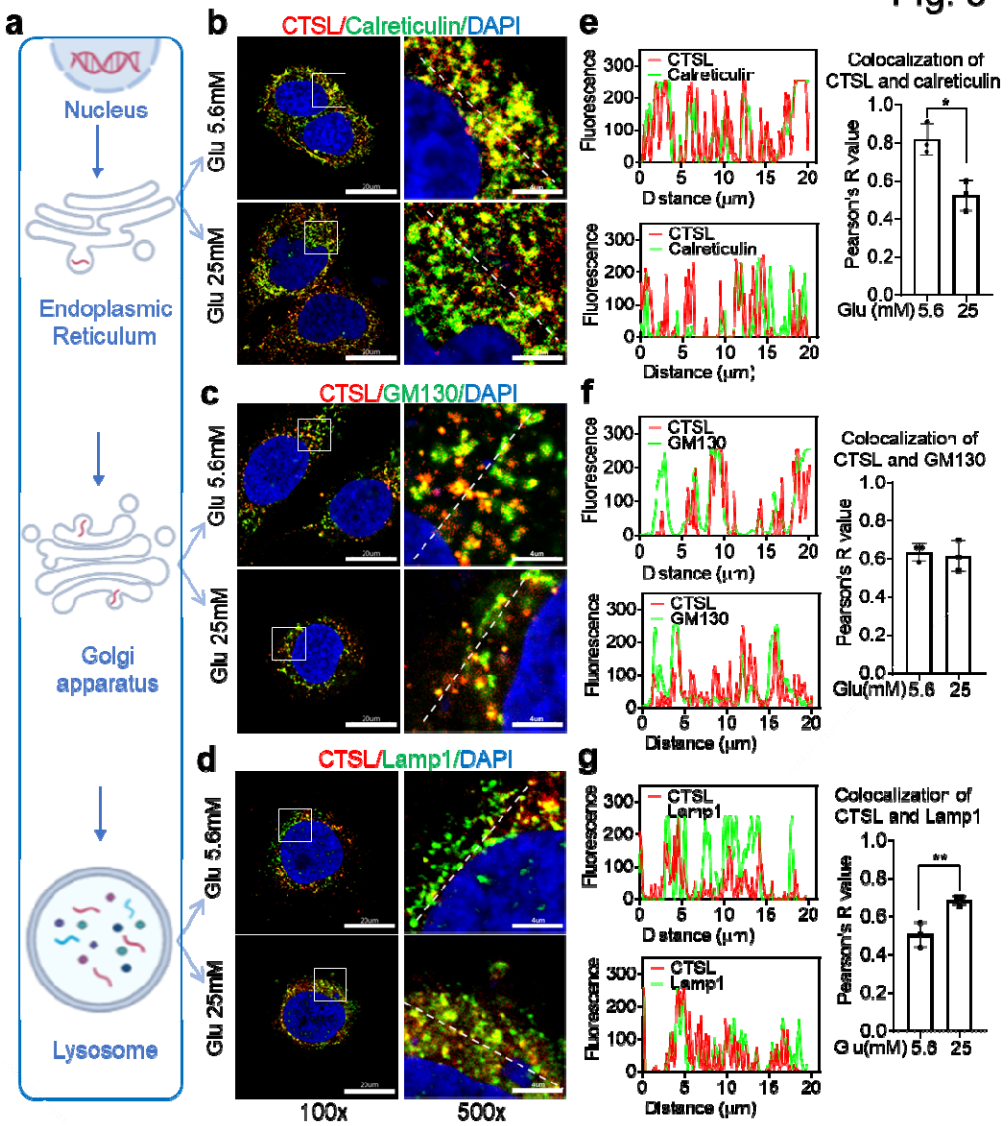
a
Nucleus
Endoplasmic Reticulum
Golgi apparatus
Lysosome
b
CTSL/Calreticulin/DAPI
Glu 5.6mM
Glu 25mM
c
CTSL/GM130/DAPI
d
CTSL/Lamp1/DAPI
100x
500x
e
CTSL
Calreticulin
Fluorescence
Distance (μm)
Colocalization of CTSL and calreticulin
Pearson's R value
Glu (mM) 5.6 25
f
GM130
Colocalization of CTSL and GM130
g
Lamp1
Colocalization of CTSL and Lamp1

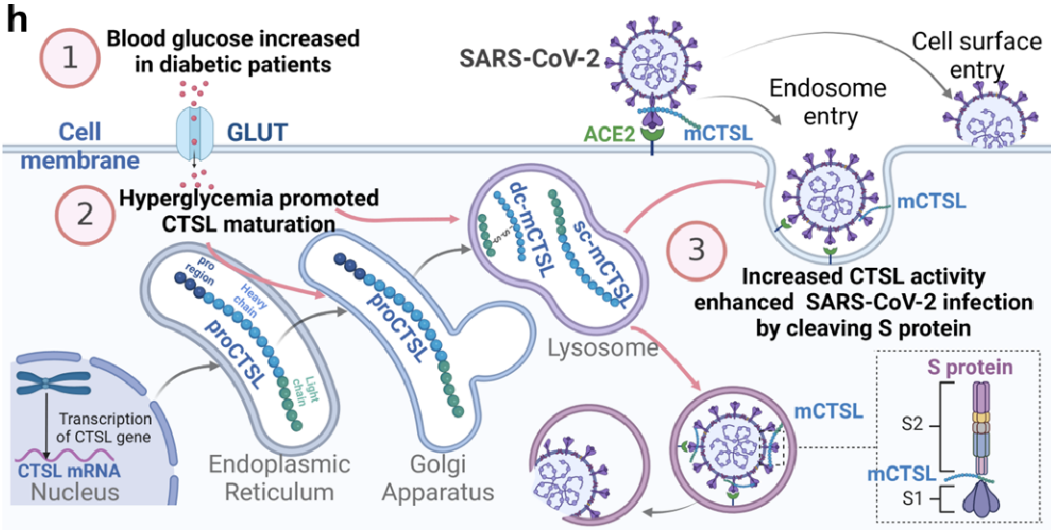
h
1
Blood glucose increased in diabetic patients
Cell membrane
GLUT
2
Hyperglycemia promoted CTSL maturation
SARS-CoV-2
ACE2
mCTSL
Endosome entry
Cell surface entry
3
Increased CTSL activity enhanced SARS-CoV-2 infection by cleaving S protein
dc-mCTSL
sc-mCTSL
proCTSL
Lysosome
Transcription of CTSL gene
CTSL mRNA
Nucleus
Endoplasmic Reticulum
Golgi Apparatus
S protein
S2
S1

Fig. 6 High glucose promotes CTSL translocation from endoplasmic reticulum to lysosome and enhances SARS-CoV-2 infection.

a A diagram illustrating the process of CTSL translocation via the endoplasmic reticulum (ER)-Golgi-lysosome axis. **b-d** Immunofluorescent staining of Huh7 cells cultured in 5.6 mM or 25 mM glucose as indicated. Co-localization analysis of CTSL (labeled red) and different organelles (labeled green) was performed using CTSL and organelle marker protein antibodies. **b** calreticulin for ER, **c** GM130 for Golgi apparatus, and **d** lamp1 for lysosome. **e-g** Fluorescence co-localization intensity analysis of the dashed line on the 500 times enlarged immunofluorescence picture. Fluorescence co-localization intensity was calculated using the Plot Profile tool in Image J software (n = 3). Scale bars, 20 μm for 100 x and 4 μm for 500 x. **h** Proposed mechanisms of hyperglycemia drives CTSL maturation and enhances SARS-CoV-2 infection. (1) Blood glucose increased in diabetic patients. (2) Hyperglycemia promoted CTSL maturation through the ER-Golgi-lysosome axis. (3) CTSL activity increased and facilitated SARS-CoV-2 entry, by cleaving the spike protein (consist of S1 and S2 subunits), and enhanced COVID-19 severity in diabetic patients. All statistical significance was assessed using Mann-Whitney U-test. The data are presented as the means ± SEM. *P < 0.05, **P < 0.01.

Supplementary information for

Hyperglycemia-induced cathepsin L maturation: Implications for diabetic comorbidities and COVID-19 susceptibility

Qiong He[1,*], Miao-Miao Zhao[1,*✉], Ming-Jia Li[1], Xiao-Ya Li[1], Jian-Min Jin[2,3], Ying-Mei Feng[4], Li Zhang[5], Wei-Jin Huang[5], Fang-Yuan Yang[1], and Jin-Kui Yang[1✉]

[1]Department of Endocrinology, Beijing Diabetes Institute, Beijing Tongren Hospital, Capital Medical University, Beijing, China

[2]Department of Respiratory and Critical Care Medicine, Beijing Tongren Hospital, Capital Medical University, Beijing, China

[3]Department of Internal Medicine, Union Hospital, Tongji Medical College, Huazhong University of Science and Technology, Wuhan 430022, China.

[4]Department of Science and Technology, Beijing Youan Hospital, Capital Medical University, Beijing, China

[5]Division of HIV/AIDS and Sex-Transmitted Virus Vaccines, Institute for Biological Product Control, National Institutes for Food and Drug Control (NIFDC), Beijing, China

[*]These authors contributed equally.

✉Correspondence to Jin-Kui Yang (jkyang@ccmu.edu.cn) or Miao-Miao Zhao (mmzhao@ccmu.edu.cn).

Supplementary Fig. 1

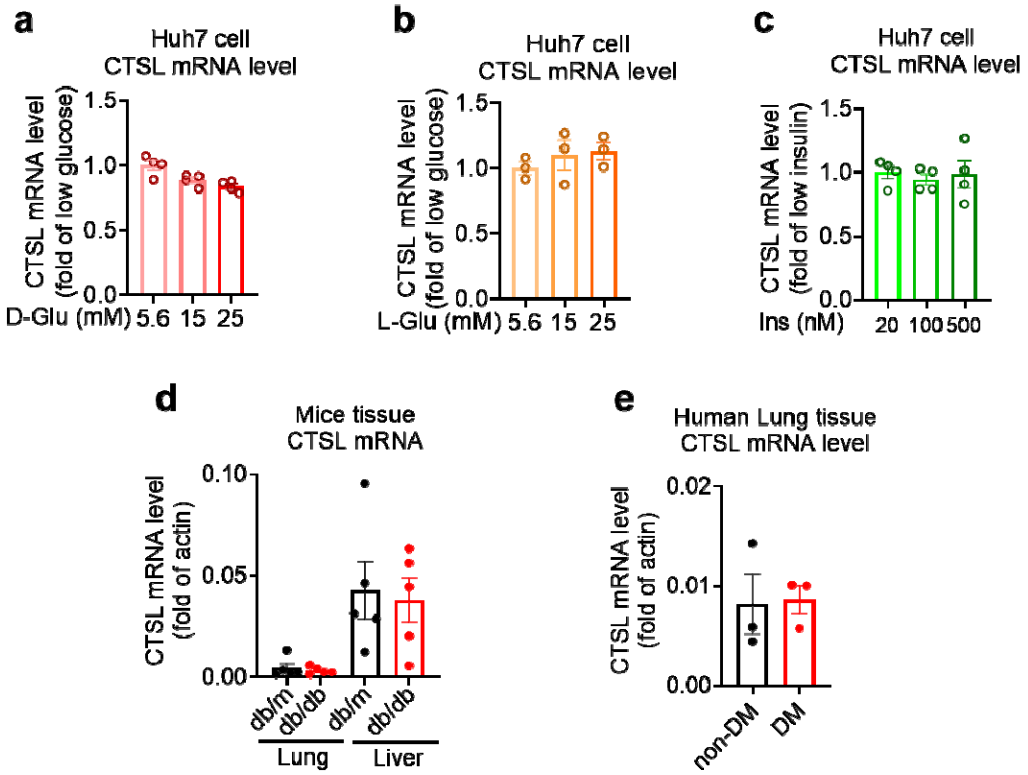

Fig. S1 CTSL mRNA levels remain unchanged under different glucose conditions.

a-**c** mRNA levels of CTSL in Huh7 cells cultured in media containing different concentrations of **a** D-glucose, **b** L-glucose, and **c** insulin, as indicated (n = 3-4). **d** mRNA levels of CTSL in db/db and db/m mouse lung and liver tissues (n = 5). **e** mRNA levels of CTSL in human lung tissues (n = 3). Significance was assessed by one-way ANOVA with Tukey's post hoc test (**a**-**c**) and Mann-Whitney U-test (**d** and **e**). The data are presented as the means ± SEM.

Supplementary Fig. 2

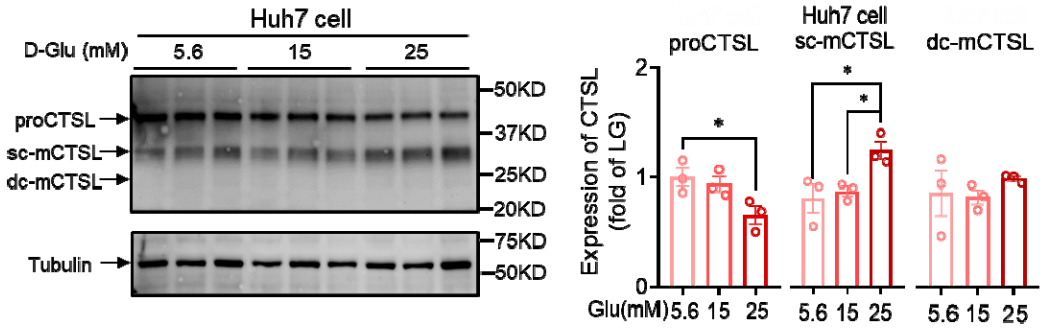

Fig. S2 CTSL protein expression in Huh7 cells under different D-glucose concentrations. CTSL expression in Huh7 cells cultured in media containing different concentrations of D-glucose (n = 3). Statistical significance was assessed by one-way ANOVA with Tukey's post hoc test. The data are presented as the means ± SEM. *P < 0.05.

Supplementary Fig. 3

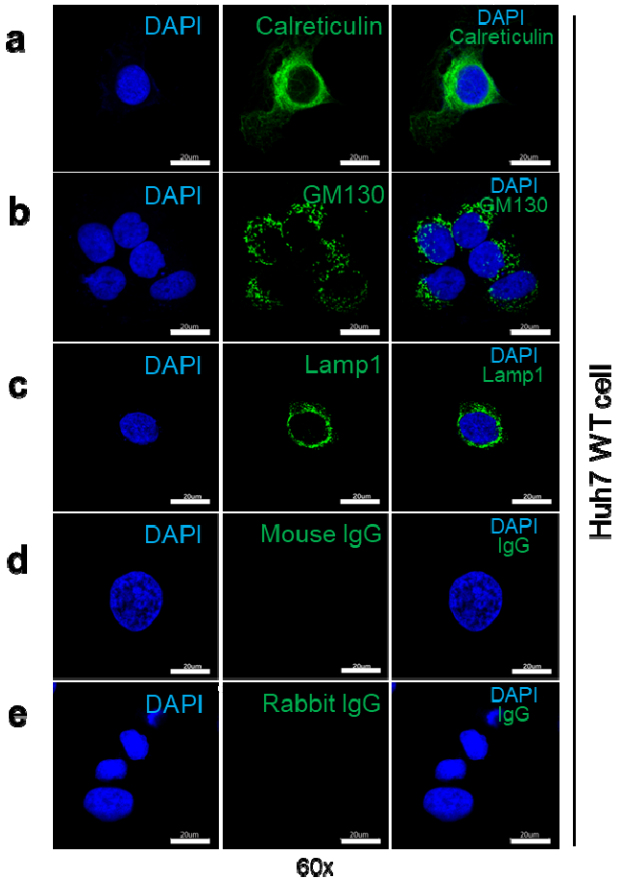

Fig. S3 Immunofluorescent staining of organelle markers representing the endoplasmic reticulum (ER), Golgi apparatus and lysosome.

a Expression of calreticulin (endoplasmic reticulum marker protein) in WT Huh7 cells. **b** Expression of GM130 (Golgi apparatus marker protein) in WT Huh7 cells. **c** Expression of Lamp1 (lysosome marker protein) in WT Huh7 cells. **d** Mouse immunoglobulin G (IgG) was used as a negative control to show the specificity of the primary antibody binding to GM130 and Lamp1 antigen. **e** Rabbit IgG was used as a negative control to show the specificity of the primary antibody binding to calreticulin antigen.

Supplementary Fig. 4

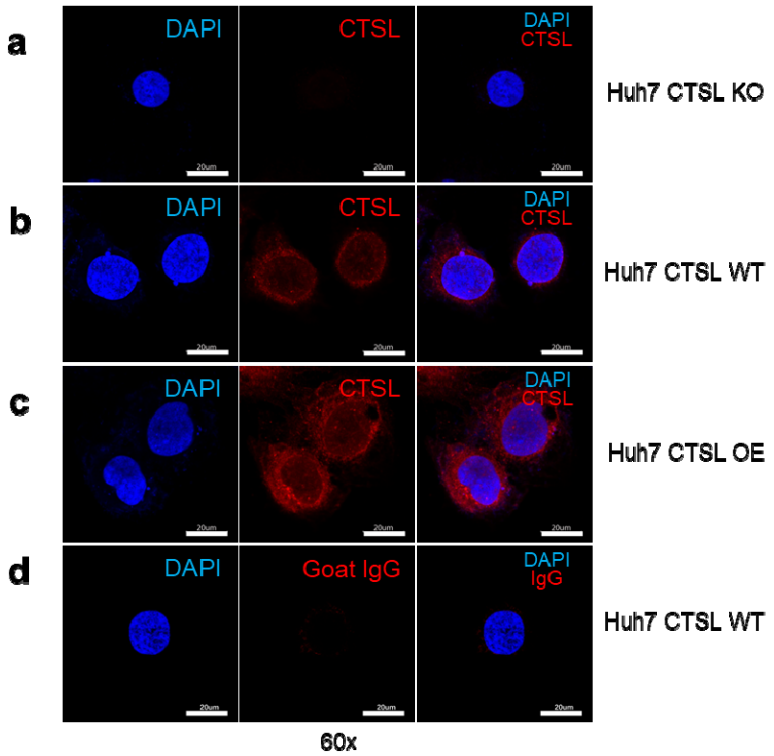

Fig. S4 Immunofluorescent staining of CTSL in Huh7 cells.

a CTSL expression in wild-type (WT) Huh7 cells. **b** CTSL expression in *CTSL* knockout (KO) Huh7 cells. **c** CTSL expression in overexpression (OE) Huh7 cells. **d** Goat IgG was used as a negative control to show the specificity of the primary antibody binding to CTSL antigen.

Supplemenary Table 1 Comparation of clinical features of COVID-19 patients

	All patients (n = 62)	**COVID-19**		
		DM (n = 31)	Non-DM (n = 31)	*P* value
Age—years	60 (52-67)	57 (51-65)	61 (56-70)	0.212†
Male—n (%)	31 (50%)	19 (61.3%)	12 (38.7%)	0.075#
Hemoglobin—g/L	129 (117-142)	123 (114-135)	135 (120-145)	0.090†
Platelet count— × 10^9/L	211 (186-289)	205 (161-278)	221 (206-293)	0.109†
White blood cell count— × 10^9/L	6.04 (4.60-7.94)	6.09 (4.82-8.03)	5.95 (4.47-7.70)	0.469†
Neutrophil percent—%	71.6 (65.6-84.4)	77.6 (67.5-89.0)	68.2 (65.3-73.5)	**0.007**†
Lymphocyte percent—%	18.7 (11.4-27.2)	14.5 (7.0-21.0)	21.7 (17.1-28.1)	**0.006**†
Potassium—mmol/L	4.03 (3.55-4.41)	3.98 (3.52-4.38)	4.04 (3.58-4.43)	0.897†
Sodium—mmol/L	138.8 (135.7-141.4)	136.3 (135.0-140.3)	139.8 (138.1-142.0)	**0.005**†
Chloride—mmol/L	102.5 (99.1-105.4)	100.7 (98.3-104.2)	104.2 (100.8-106.0)	**0.029**†
Albumin—g/L	29.4 (27.3-35.0)	28.5 (25.6-34.1)	31.6 (27.6-35.7)	0.202†
Albumin/Globulin ratio	0.90 (0.70-1.27)	0.83 (0.70-1.08)	1.05 (0.80-1.33)	**0.013**†
C-reactive protein—mg/L	29.0 (4.1-70.8)	53.4 (16.1-91.9)	11.3 (2.0-40.3)	**0.012**†
Procalcitonin—mg/L	0.08 (0.05-0.16)	0.12 (0.07-0.23)	0.06 (0.04-0.10)	**0.013**†
Alanine aminotransferase—U/L	38 (24-50)	40 (28-53)	34 (22-44)	0.105†
Aspartate aminotransferase—U/L	31 (22-47)	34 (27-52)	29 (19-40)	**0.037**†
Creatine kinase–MB—ng/mL	0.44 (0.21-0.88)	0.75 (0.43-1.68)	0.32 (0.18-0.63)	**0.006**†
Myoglobin—g/L	47.1 (28.0-75.0)	60.4 (39.4-129.5)	33.5 (26.1-51.9)	**0.002**†
Blood urea nitrogen—mmol/L	5.03 (3.41-6.78)	5.79 (4.31-7.49)	4.10 (3.11-5.47)	**0.019**†
Creatinine—μmol/L	68.3 (56.9-86.6)	74.0 (60.0-94.2)	63.5 (52.2-73.4)	**0.017**†

Data are median (IQR) or n (%). *P* values were calculated by Mann-Whitney *U*-test (†) or χ^2 test (#), as appropriate for group comparison analyses.

Supplemenary Table 2 Demographic and clinical characteristics of non-COVID-19 patients

	All individuals N = 122	**Non-COVID-19**		
		Healthy N = 61	DM N = 61	*P*
Age—years	59 (55-62)	58 (55-64)	60 (58-62)	0.141†
Male—n (%)	58 (47.5%)	27 (44.3%)	31 (50.8%)	0.468#
BMI	25.01 (22.37-27.34)	24.8 (22.2-26.7)	25.4 (22.8-27.5)	0.347†
HbA1c—%	5.85 (5.30-7.13)	5.4 (5.2-5.8)	7.0 (6.2-8.2)	**0.000†**
CTSL conc. —pg/mL	1637.0 (1337.8-2120.9)	1535.4 (1251.3-1838.7)	1715.7 (1408.0-2261.4)	**0.009†**
CTSL activity—RLU	1708.0 (477.2-3058.7)	477.2 (429.8-601.8)	3050.0 (2534.0-3713.0)	**0.000†**

Data are median (IQR) or n (%). *P* values were calculated by Mann-Whitney *U*-test (†) or χ^2 test (#), as appropriate for group comparison analyses.

Supplemenary Table 3 Nonparametric correlations of parameters correlated with CTSL levels and diabetes in non-COVID-19 individuals

	CTSL activity	CTSL conc	HbA1c	BMI	Systolic pressure	Diastolic pressure	Waist	Hip	WHR	LDL	Serum CREA	Age	Gender	Diabetes	HBP	CHD
CTSL activity	1.00															
CTSL conc	**0.248 (0.006)**	1.00														
HbA1c	**0.565 (0.000)**	**0.263 (0.003)**	1.00													
BMI	0.162 (0.084)	0 (0.997)	0.134 (0.152)	1.00												
Systolic pressure	**0.314 (0.001)**	**0.415 (0.000)**	**0.294 (0.002)**	0.182 (0.056)	1.00											
Diastolic pressure	**-0.235 (0.012)**	0.048 (0.613)	-0.124 (0.190)	**0.232 (0.014)**	**0.213 (0.023)**	1.00										
Waist	0.045 (0.634)	0.075 (0.421)	0.139 (0.138)	**0.728 (0.000)**	**0.204 (0.031)**	**0.191 (0.044)**	1.00									
Hip	**-0.246 (0.008)**	-0.023 (0.809)	-0.038 (0.688)	**0.572 (0.000)**	0.120 (0.208)	**0.284 (0.002)**	**0.678 (0.000)**	1.00								
WHR	**0.385 (0.000)**	0.115 (0.222)	**0.241 (0.009)**	**0.331 (0.000)**	**0.198 (0.037)**	-0.031 (0.744)	**0.525 (0.000)**	-0.157 (0.093)	1.00							
LDL	**-0.264 (0.003)**	0.066 (0.468)	-0.058 (0.526)	-0.011 (0.903)	-0.090 (0.339)	**0.202 (0.031)**	0.007 (0.941)	0.089 (0.342)	-0.098 (0.295)	1.00						
Serum CREA	-0.096 (0.291)	**0.189 (0.037)**	-0.102 (0.262)	0.041 (0.664)	0.071 (0.450)	0.103 (0.277)	0.177 (0.058)	0.131 (0.163)	0.070 (0.458)	-0.066 (0.467)	1.00					
Age	**0.205 (0.023)**	**0.261 (0.004)**	**0.233 (0.010)**	0.028 (0.762)	**0.211 (0.024)**	-0.065 (0.492)	0.085 (0.362)	0.045 (0.631)	0.122 (0.196)	0.065 (0.479)	-0.046 (0.618)	1.00				
Gender	0.061 (0.504)	**0.322 (0.000)**	0.023 (0.801)	-0.028 (0.768)	0.086 (0.365)	0.077 (0.416)	0.148 (0.112)	0.081 (0.392)	0.094 (0.317)	-0.142 (0.118)	**0.528 (0.000)**	**0.217 (0.016)**	1.00			
Diabetes	**0.866 (0.000)**	**0.239 (0.008)**	**0.669 (0.000)**	0.088 (0.350)	**0.348 (0.000)**	**-0.221 (0.018)**	-0.003 (0.978)	**-0.309 (0.001)**	**0.389 (0.000)**	**-0.270 (0.003)**	-0.046 (0.618)	**0.254 (0.005)**	0.066 (0.472)	1.00		
HBP	**0.676 (0.000)**	**0.188 (0.038)**	**0.593 (0.000)**	0.174 (0.063)	**0.397 (0.000)**	-0.131 (0.164)	0.077 (0.414)	-0.167 (0.075)	**0.303 (0.001)**	**-0.214 (0.018)**	-0.087 (0.342)	**0.233 (0.010)**	-0.057 (0.532)	**0.829 (0.000)**	1.00	
CHD	**0.445 (0.000)**	**0.179 (0.049)**	**0.350 (0.000)**	**0.265 (0.004)**	**0.265 (0.004)**	-0.037 (0.699)	**0.200 (0.031)**	-0.040 (0.672)	**0.383 (0.000)**	-0.164 (0.071)	0.090 (0.324)	**0.214 (0.018)**	0.046 (0.615)	**0.533 (0.000)**	**0.579 (0.000)**	1.00

Data are correlation coefficient (*P* value). Spearman's rho test (two-tailed).

Supplemenary Table 4: Demographic and clinical characteristics of human lung tissues donor

	No.	Gender	Age range*	Glucose-mmol/L	LDL-C-mmol/L
DM	1	Male	46-50	5.2	3.31
	2	Female	46-50	5.6	2.49
	3	Male	66-70	8	2.45
Non-DM	4	Male	41-45	6	1.64
	5	Female	26-30	5.2	3.98
	6	Male	41-45	4.2	4.28

* The identifying information has been substituted with a range.

Six enrolled patients undergoing lung surgery in general surgery department of Beijing Tongren Hospital ranging from March to June, 2022.

Supplemenary Table 5 List of oligonucleotide primer pairs used in real time RT-PCR analysis

Primer	Species	Forward (5'-3')	Reverse (5'-3')
CTSL	human	AAACTGGGAGGCTTATCTCACT	GCATAATCCATTAGGCCACCAT
CTSL	mouse	CTACACAACGGGGAATACAGC	CATTGGTCATGTCACCGAAGG
β-actin	human	TCATGAAGTGTGACGTGGACATC	CAGGAGGAGCAATGATCTTGATCT
β-actin	mouse	GTGACGTTGACATCCGTAAAGA	GCCGGACTCATCGTACTCC

Supplemenary Table 6 Specific Antibodies for Western blotting and Immunofluorescence assa

Protein	Company	Catalog	Source
CTSL	R&D System	AF952	Goat IgG
α-tubulin	Proteintech	66031-1-Ig	Mouse IgG
β-actin	Proteintech	66009-1-Ig	Mouse IgG
Calreticulin	Cellsignal	112238	Rabbit IgG
GM130	BD Biosciences	610822	Mouse IgG
Lamp1	PTM BIO	PTM-5775	Mouse IgG
Goat IgG	Beyotime	A7007	Goat IgG
Rabbit IgG	Beyotime	A7016	Rabbit IgG
Mouse IgG	Beyotime	A7028	Mouse IgG